*Materials Science Forum*
*ISSN: 1662-9752, Vol. 1192, pp 97-103*
*doi:10.4028/p-t0ptSI*

*Submitted: 2025-09-26*
*Revised: 2025-12-26*
*Accepted: 2026-02-26*
*Online: 2026-05-20*

# Analysis of Backside Metal Contact Resistance on Low-Resistivity Polycrystalline in 4H-SiC-Bonded Substrates

M. Kobayashi[1,a*], S. Ishikawa[2,b], Y. Higashi[2,c], H. Sezaki[3,d], M. Okamoto[2,e], S. Harada[2,f] and K. Kojima[2,g]

[1]Sumitomo Metal Mining Co., Ltd., 5-11-3, Shimbashi, Minato-ku, Tokyo 105-0004, Japan

[2]Advanced Power Electronics Research Center, National Institute of Advanced Industrial Science and Technology (AIST), Tsukuba, Ibaraki 305-8568, Japan

[3]PHENITEC SEMICONDUCTOR Corp., 6833, Kinoko-cho, Ibara, Okayama 715-8602, Japan

[a*]motoki.kobayashi.x2@smm-g.com, [b]ishikawa-seiji@aist.go.jp, [c]higashi-phenitec@aist.go.jp, [d]hiroshi-sezaki@phenitec.co.jp, [e]mitsuo-okamoto@aist.go.jp, [f]s-harada@aist.go.jp, [g]kazu-kojima@aist.go.jp

**Keywords:** bonded substrate, low-resistivity polycrystalline layer, backside contact resistance, SIMS, hall measurement, circular TLM, threshold resistivity.

**Abstract.** In this study, 4H-SiC bonded substrates (bonded-SiC) with an average resistivity of 2.4–31.5 mΩ·cm were prepared, and attention has been directed toward the relationship between the resistivity of bonded-SiC and the contact resistance at the backside where metal Ti/Ni was applied. A circular transmission line model (cTLM) was used to accurately measure the backside contact resistance. A linear correlation was found between $\rho_C$ and the resistivity of bonded-SiCs at room temperature (RT). This result indicates the existence of a threshold resistivity at which the specific contact resistance ($\rho_C$) in the range of $2.2 \times 10^{-6}$ to $1.5 \times 10^{-5}$ Ω·cm$^2$ can be achieved without contact annealing; it also indicates that the temperature dependence of $\rho_C$ between 17.4 and 34.4 mΩ·cm of the resistivity on bonded-SiCs is eliminated. This phenomenon can occur because $\rho_C$ is dominated by tunneling current above the nitrogen concentration at the threshold resistivity, which is driven by the high nitrogen concentration and sufficient carrier activation in the polycrystalline portion (polycrystalline layer) of bonded-SiCs. These are important properties resulting from a polycrystalline layer with a 3C structure in bonded-SiC.

## Introduction

The 4H-SiC bonded-SiC (SiCkrest™) consists of a thin monocrystalline 4H-SiC layer with a thickness of less than 1 μm, which is bonded to an n-type low-resistivity polycrystalline 3C-SiC substrate via surface-activated bonding. Fig. 1 shows (a) the photogram and (b) the schematic structure of SiCkrest™. Some features of this substrate, for example, no unstable interlayer at bonded interface, which is shown in this cross-sectional transmission electron microscope (TEM) image, enables to apply various high temperature process of SiC. And the polycrystalline layer exhibits a low resistivity of under 10 mΩ·cm, which is significantly lower than that of the 4H-SiC monocrystalline substrate. This hybrid structure can be applied to the same epitaxial growth and device processes as conventional 4H-SiC bulk substrates [1, 4]. In addition, compared with traditional 4H-SiC bulk substrates, it has reduced on-state resistance [1] and suppressed forward bias degradation in PiN diodes [2, 3] and a significant decrease in switching loss within the body-diode of MOSFETs [4].

In a previous study, this low-resistivity bonded-SiC not only reduced the on-resistance of SBD but also provided a low-resistance backside contact without the need for contact annealing and reduced temperature dependence [5]. However, the effect of resistivity on the necessity for contact annealing and the temperature dependence of $\rho_C$ remains unclear because the resistivity of the bonded-SiCs tested in our previous research was only 10 mΩ·cm. In this study, bonded-SiCs with an average resistivity ranging from 2.4 to 31.5 mΩ·cm were prepared, and attention has been directed toward the relationship between the resistivity of the bonded-SiC and the contact resistance at the grinded

backside where metal Ti/Ni was applied. A cTLM was used to accurately measure the contact resistance. The relationship between the resistivity of the bonded-SiC and the backside contact resistance was clarified, and the mechanism underlying such a relationship was investigated.

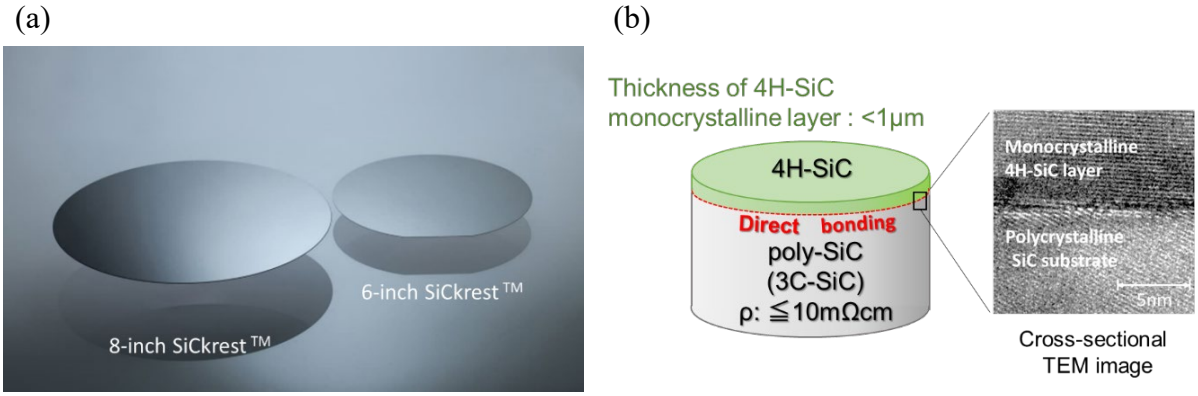


**Fig. 1.** (a) the photogram and (b) the schematic structure of SiCkrest™ and TEM image of bonded interface.

## Experimental

Fig. 2 presents the resistivity of the bonded-SiCs prepared in this study, which possessed an average resistivity ranging from 2.4 to 31.5 mΩ·cm compared with 10 mΩ·cm of the previous study. The polycrystalline layer of the bonded-SiCs with different resistivities was prepared by changing the nitrogen concentration through chemical vapor deposition. he resistivity of the bonded-SiCs was evaluated by using Eddy current measurements, whereas the nitrogen concentration in the polycrystalline layer was analyzed by using secondary-ion mass spectrometry (SIMS), and the carrier concentration was determined through Hall measurements, as shown in Fig. 3 (a). Fig. 3 (b) shows the measurement position within a substrate of the resistivity, nitrogen concentration, and carrier concentration. Resistivity and $\rho_C$ were measured at 37 points across the entire surface and five points, respectively. Other analyses were performed at the same position (see Fig. 3 (b)) within the substrate for accurate comparison.

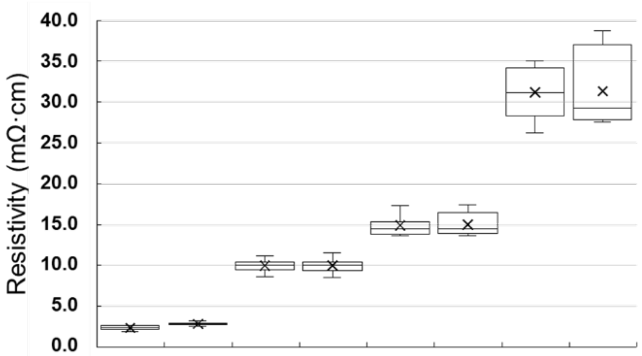


| Bonded-SiC sample No. | 1 | 2 | 3 | 4 | 5 | 6 | 7 | 8 |
|---|---|---|---|---|---|---|---|---|
| AVERAGE | 2.35 | 2.84 | 9.97 | 9.99 | 14.90 | 14.99 | 31.21 | 31.52 |
| MAX | 2.66 | 3.23 | 11.15 | 11.54 | 17.83 | 17.42 | 35.00 | 39.01 |
| MIN | 1.87 | 2.50 | 8.64 | 8.55 | 13.60 | 13.65 | 26.25 | 27.57 |
| σ | 0.23 | 0.18 | 0.65 | 0.73 | 1.24 | 1.23 | 2.63 | 4.41 |

**Fig. 2.** Resistivity of the bonded-SiCs prepared in this study.

(a)

| Item | Method | Location |
|---|---|---|
| Resistivity of substrate | Eddy current measurement | 37points / Full substrate |
| Specific contact resistance ($\rho_C$) of backside | IV measurement of cTLM | 1 |
| Nitrogen concentration in polycrystalline layer | SIMS | 2 |
| Carrier concentration in polycrystalline layer | Hall measurement | 2 |

(b)

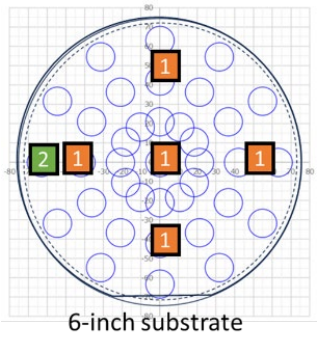


**Fig. 3.** (a) Evaluation items and methods for bonded-SiCs and polycrystalline layers. (b) Measurement position within a substrate in this study.

cTLM was used to accurately measure the $\rho_C$ [6, 7]. Fig. 4 illustrates (a) the process flow, (b) schematic structure, and (c) a split table of the cTLM samples. Three types of samples were tested in this study: (1) 4H-SiC monocrystalline substrate (mono-SiC) with contact annealing, (2) bonded-SiCs with contact annealing, and (3) bonded-SiCs without contact annealing. I–V measurements were conducted using an Agilent 4156C, with the temperature controlled at RT, 75°C, 125°C, and 175°C using a hot plate.

(a)

- Prepare Bonded substrate
  (Use the grinded back side)
  **A) Bonded-SiC 2.4-32mΩ·cm**
  **B) Mono-SiC 20mΩ·cm**
- Field Oxidation
- Ohmic Metal: Ti/Ni
- RTA, 1200 ℃ :
  (c) **Split table**
- Top Metal: Al 3μm
- IV measurement
  - Apparatus : Agilent 4156C
  - Temperature : RT, 75, 125, 175℃ (Hot Plate)
  - Temperature control method: TC

(b)

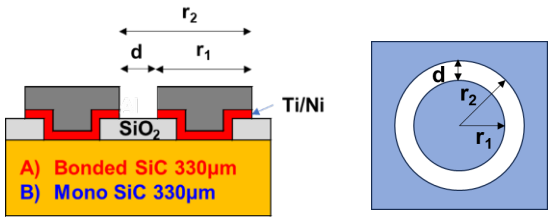


(c)

| | (1) Mono-SiC | (2) Bonded-SiC | (3) Bonded-SiC wo anneal |
|---|---|---|---|
| Mono-SiC | 20mΩ·cm | 20mΩ·cm | 20mΩ·cm |
| Bonded-SiC (Sample No.) | No | 2.8-32mΩ·cm (2,4,6,8) | 2.4-31mΩ·cm (1,3,5,7) |
| RTA anneal | Yes | Yes | No |

**Fig. 4.** (a) Process flow, (b) schematic image of the cTLM structure, and (c) split table for cTLM samples in this study.

## Results and Discussion

### Relationship between the resistivity of the bonded substrate and the $\rho_C$

Fig. 5 illustrates the relationship between the resistivity of bonded-SiCs and $\rho_C$ at RT. Both measurements were conducted at the same locations on the substrate (center and four peripheral positions) to accurately investigate the correlation between resistivity and $\rho_C$. This result indicates a linear correlation between the resistivity of bonded-SiCs and $\rho_C$ when the resistivity is 17.4 mΩ·cm or lower at RT. Even without contact annealing, at the lowest resistivity point in the substrate, the resistivity of the bonded-SiC is 1.9 mΩ·cm, whereas $\rho_C$ is approximately $2.2 \times 10^{-6}$ Ω·cm$^2$ at RT, which is equivalent to an ohmic contact to a mono-SiC using $n^+$ doping and high-temperature annealing [6]. Furthermore, as indicated by the symbols ■ and ● for $\rho_C$ without and with annealing, respectively, no difference in $\rho_C$ between the two was observed for any resistivity values of

17.4 mΩ·cm or less. However, for resistivity values exceeding 17.4 mΩ·cm, $\rho_C$ increased and varied across the substrate without contact annealing.

Fig. 6 shows the distribution of $\rho_C$ within a substrate (Fig. 5 (a) and (b)). Bonded-SiCs with resistivities of approximately 17 and 34 mΩ·cm showed minimal variations in $\rho_C$ with annealing. By contrast, bonded-SiCs with a resistivity near 34 mΩ·cm without annealing exhibited a significant variation in $\rho_C$ similar to mono-SiC because of unstable silicide formation with a backside metal.

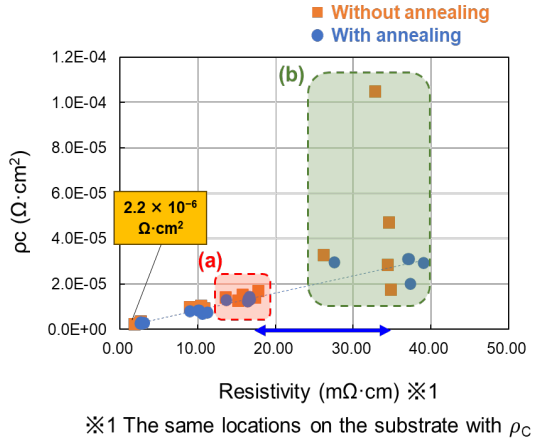


**Fig. 5.** Relationship between the resistivity of bonded-SiCs and $\rho_C$ at RT. The symbols ■ and ● indicate $\rho_C$ without and with annealing, respectively.

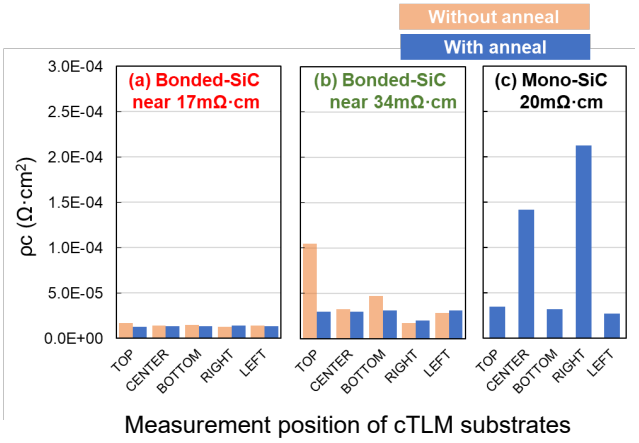


**Fig. 6.** Distribution within a substrate of $\rho_C$: (a) bonded-SiCs with a resistivity near 17 mΩ·cm, as plotted in Fig. 5 (a); (b) bonded-SiCs with a resistivity near 34 mΩ·cm, as plotted on Fig. 4 (b); and (c) mono-SiC.

Fig. 7 (a) shows the temperature dependence of $\rho_C$ for mono-SiC with annealing and bonded-SiCs without annealing, as well as for bonded-SiCs as a function of resistivity. Mono-SiC showed a strong temperature dependence in the previous study [5], whereas bonded-SiCs exhibited no temperature dependence at 17.4 mΩ·cm or less and a weak negative temperature dependence at 34.4 mΩ·cm. Fig. 7 (b) presents the relationship between the resistivity of bonded-SiCs and $\rho_C$ at RT, 175°C, and the difference ($\Delta\rho_C$) between RT and 175°C. In mono-SiC and bonded-SiCs with a resistivity of 34.4 mΩ·cm or more, $\Delta\rho_C$ indicates a negative value (negative temperature characteristic).

These results indicate the existence of a threshold resistivity at which the $\rho_C$ in the range of $2.2 \times 10^{-6}$ to $1.5 \times 10^{-5}$ Ω·cm² can be achieved without contact annealing; it also indicates that the temperature dependence of $\rho_C$ between 17.4 and 34.4 mΩ·cm is eliminated.

(a)

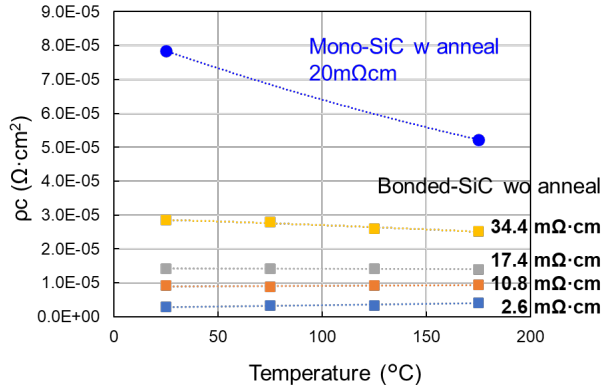


(b)

Unit : ×10⁻⁶ Ω·cm²

| Resistivity of bonded-SiC | ρc at RT | ρc at 175°C | $\Delta\rho_C$ |
|---|---|---|---|
| (Ref) Mono 20mΩ·cm | 78.5 | 52.2 | -26.3 |
| Bonded 34.4mΩ·cm | 28.5 | 25.2 | -3.3 |
| Bonded 17.4mΩ·cm | 14.1 | 14.0 | -0.001 |
| Bonded 10.8mΩ·cm | 9.2 | 9.5 | 0.3 |
| Bonded 2.6mΩ·cm | 2.9 | 4.1 | 1.2 |

**Fig. 7.** (a) Temperature dependence of $\rho_C$ of bonded-SiCs (■) and mono-SiC (●). Resistivity varies from 2.6 to 34.4 mΩ·cm for the bonded-SiCs. (b) Relationship between the resistivity of bonded-SiCs and $\rho_C$ at RT, 175°C, and the difference ($\Delta\rho_C$) between RT and 175°C.

**Analysis of a polycrystalline layer of a bonded substrate**

Fig. 8 presents the results of SIMS and Hall measurements, illustrating (a) the relationship between the resistivity of bonded-SiCs and nitrogen concentration and (b) the relationship between nitrogen concentration and carrier concentration, as compared with mono-SiC. The nitrogen concentration in bonded-SiCs correlates with the resistivity of the polycrystalline layer and is one order of magnitude higher than that in mono-SiC with similar resistivity (see Fig. 8 (a)). This is due to the low carrier mobility in the polycrystalline layer; however, it is easy to increase the nitrogen concentration by an order of magnitude in the polycrystalline layer. Furthermore, the nitrogen and carrier concentrations in the polycrystalline layer of bonded-SiCs were nearly identical, indicating that the nitrogen in the polycrystalline layer was nearly 100% activated (see Fig. 8 (b)). Yu et al. have presented the relationship between $\rho_C$ and donor concentration ($N_D$) [8], and it is known that $\rho_C$ depends on carrier concentration. Below, we discuss the effect of high carrier concentration in polycrystalline bonded SiC on $\rho_C$.

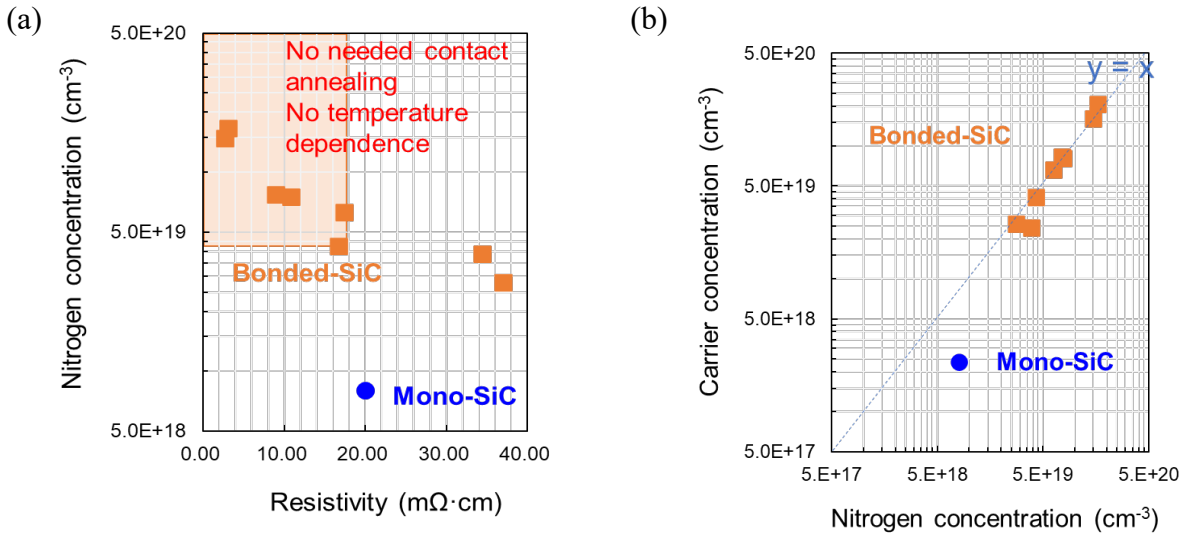


**Fig. 8.** Relationship between (a) the resistivity of bonded-SiCs and nitrogen concentration and between (b) nitrogen concentration and carrier concentration in the polycrystalline layer of bonded-SiCs as compared with mono-SiC.

Fig. 9 (a) presents the band diagram for the ohmic contact of mono-SiC as reported [6, 9]. For mono-SiC, $n^+$ doping with a concentration exceeding $1 \times 10^{19}$ cm$^{-3}$, combined with high-temperature annealing, can provide low-resistance ohmic contact to 4H mono-SiC. $n^+$ doping increases the Fermi level ($E_F$) of the mono-SiC above its conduction band energy ($E_C$), resulting in a thin Schottky barrier. Considering that the conduction between mono-SiC and a metal is dominated by tunneling current, extremely low-resistance ohmic contact can be achieved. In this case, the carrier transport mechanism is known as field emission.

Fig. 9 (b) illustrates the band diagram for a polycrystalline layer of bonded-SiC with ohmic contact, as predicted based on results in this study. As shown in Fig. 7, the $\rho_C$ of the polycrystalline layer on bonded-SiC exhibited no temperature dependence below the threshold resistivity, indicating that tunneling current is the dominant conduction mechanism between the polycrystalline layer and the backside metal. By contrast, the $\rho_C$ on mono-SiC shows temperature dependence, indicating that thermally excited current and tunneling current contribute to the conduction. In this case, the mechanism underlying current transport through the barrier is known as thermionic field emission. Similarly, above the threshold resistivity, $\rho_C$ of the polycrystalline layer on bonded-SiC exhibits temperature dependence, indicating that thermally excited current becomes dominant alongside tunneling current in the conduction between the polycrystalline layer and the backside metal.

Furthermore, a linear correlation exists between the resistivity of bonded-SiCs and $\rho_C$ below the threshold resistivity (Fig. 5). Similar to the mechanism underlying the ohmic contact of mono-SiC

(Fig. 9 (a)), a high nitrogen concentration in the polycrystalline layer leads to a thinner barrier width and increased tunneling current. Thus, $\rho_C$ is primarily determined by the resistivity of the polycrystalline layer of bonded-SiC. Considering that $\rho_C$ is primarily governed by $N_D$ and barrier height ($\phi_B$) [8], when tunneling current dominates the ohmic contact, the current depends on $N_D$. In addition, the polycrystalline layer has a high nitrogen concentration (Fig. 8), with nearly 100% activation, resulting in a carrier concentration of $1.5 \times 10^{20}$ cm$^{-3}$ (at a resistivity of 2.6 mΩ·cm). This value is an order of magnitude higher than the $n^+$ doping concentration required for mono-SiC tunnel ohmic contacts ($\geq 1 \times 10^{19}$ cm$^{-3}$). Therefore, the $E_F$ value of the polycrystalline layer can be close to or above $E_C$, which is similar to the band structure of $n^+$ doped mono-SiC ohmic contact [6]. Under these conditions, a large number of electrons exist above the conduction band, which could be a key factor that increases tunneling current. These results also support that, above the nitrogen concentration at the threshold resistivity, tunneling current is the dominant conduction mechanism between the polycrystalline layer and the backside metal.

As shown in Fig. 9, by simplifying the equation presented by Yu et al. [8], $\rho_C$ is proportional to $\exp\left(\phi_B / \sqrt{N}\right)$. In order to analytically model a linear relationship between $\rho_C$ and resistivity of the polycrystalline layer of bonded-SiC, it is necessary to clarify the relationship between carrier concentration and resistivity; however, this has not yet been achieved. Additionally, the formation of Ti/Ni silicide in the backside contact affects both the $\phi_B$ at the silicide interface and the thickness of the natural oxide layer (tunneling distance) at the interface. However, since the contact between the polycrystalline layer and Ti/Ni is ohmic, it is difficult to measure the barrier height, and thus the influence of $\phi_B$ has not been separated. These remain issues to be addressed in future work.

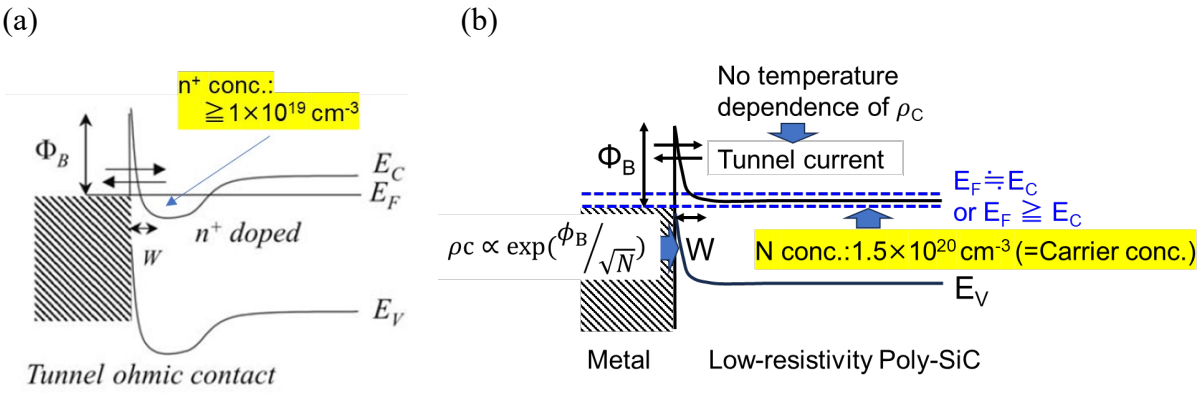


**Fig. 9.** Band diagrams of the (a) tunnel ohmic contact of 4H-SiC using $n^+$ doping and the high-temperature annealing [6] and (b) ohmic contact of 3C-SiC polycrystalline with a backside metal.

## Summary

In this study, bonded-SiCs (SiCkrest™) with an average resistivity of 2.4–31.5 mΩ·cm were prepared. The relationship between the resistivity of the bonded-SiCs and the backside contact resistance was clarified, and the mechanism underlying such a relationship was investigated.

In the polycrystalline layer of bonded-SiC, the correlation between the resistivity of bonded-SiCs and $\rho_C$ indicates the existence of a threshold resistivity at which low $\rho_C$ can be achieved without contact annealing; it also indicates that the temperature dependence of $\rho_C$ is eliminated. This phenomenon is attributed to the dominance of tunneling current above the nitrogen concentration at the threshold resistivity, which is driven by a high nitrogen concentration and sufficient carrier activation in the polycrystalline layer of bonded-SiCs. These are important properties resulting from a polycrystalline layer with a 3C structure in bonded-SiC.

**Acknowledgments**

This paper was produced as part of a joint research project of Tsukuba Power Electronics Constellations. The co-authors, S. Ishikawa and Y. Higashi, are affiliated with PHENITEC Semiconductor Corp.

**References**

[1] T. Shimono, H. Uchida, A. Onogi and H. Fujiwara, presented at the 7th Meeting on Advanced Power Semiconductors, Japan (2020).

[2] N. Hatta, S. Ishikawa, K. Ozono, K. Masumoto, K. Yagi, M. Kobayashi, S. Kurihara, S. Harada and K. Kojima, Key Engineering Materials 948, p. 107 (2023).

[3] H. Uchida, M. Kobayashi, N. Hatta, S. Ishikawa, K. Ozono, K. Masumoto, S. Kurihara, S. Harada and K. Kojima, Abstract of 20th ICSCRM, p. 209 (2023).

[4] Y. Higashi, S. Ishikawa, K. Ozono, M. Kobayashi, H. Uchida, M. Okamoto, S. Harada, K. Kojima, T. Kato and Y. Tanaka, Scientific Books of Abstracts, 8, 12-13, 2024.

[5] M. Kobayashi, H. Uchida, N. Hatta, S. Ishikawa, Y. Higashi, H. Sezaki, S. Harada and K. Kojima, Scientific Books of Abstracts, 8, 396-398, 2024.

[6] F. Roccaforte, F. La Via and V. Raineri, International Journal of High Speed Electronics and Systems, 15, 77-116, 2006.

[7] G.K. Reeves, Solid-State Electron, 23, 487-490, 1980.

[8] Y. Liu, S. P. Singh, L. M. Kyaw, M. K. Bera, Y. J. Ngoo, H. R. Tan, S. Tripathy, G. Q. Lo, and E. F. Chora, ECS Journal of Solid State Science and Technology, 4, 30-35, 2015.

[9] K. Maeda, K. Kuwahara, M. Hara, M. Kaneko and T. Kimoto, Scientific Books of Abstracts, 8, 402-404, 2024.